

# Electronic Supplementary Information

## Plasmonically Enhanced Electromotive Force of Narrow Band Gap PbS QDs Based Photovoltaics

Xiaowei Li,<sup>a</sup> Paul D. McNaughten,<sup>b</sup> Paul O'Brien,<sup>b, c</sup> Hiro Minamimoto,<sup>a</sup>

and Kei Murakoshi\*<sup>a</sup>

<sup>a</sup>Department of Chemistry, Faculty of Science, Hokkaido University, Sapporo, 060-0810, Japan

<sup>b</sup>School of Chemistry, the University of Manchester, Oxford Road, Manchester, M13 9PL, United Kingdom

<sup>c</sup>School of Materials, the University of Manchester, Oxford Road, Manchester, M13 9PL, United Kingdom

### Chemicals used in PbS quantum dot synthesis

Lead (II) oxide ( $\geq 99\%$ , Aldrich), oleic acid (90%, Alfa-Aesar), bis(trimethylsilyl)sulphide (99.9%, Aldrich) and 1-octadecene (90%, Aldrich).

### Preparation of lead sulfide quantum dots

Table S1 Growth temperatures and times used to synthesise the different sized PbS QDs

PbS QDs	Temperature (°C)	time (s)
OP-728	100	80
OP-1101	150	30
OP-1344	200	30

### Quantities analysis of PbS QDs

We analyzed the quantity of lead in the colloidal dispersion of PbS QDs via inductively coupled plasma atomic emission spectroscopy (ICPE-9000, SHIMADZU). The as synthesized PbS QDs dispersed in hexane were added into ethanol and centrifuged to dissolve oleic acid, as organics cool the plasma. Then the supernatant was removed and evaporated. The dried QDs were digested in dilute nitric acid to form  $\text{Pb}(\text{NO}_3)_2$  by accompanied with  $\text{H}_2\text{S}$  gas, as  $\text{HNO}_3$  in a high concentration generates solid S or  $\text{PbSO}_4$  that would clog the nebulizer and thus underestimate the quantity of Pb.<sup>1</sup>

Lead nitrate dissolved in dilute nitric acid was used as the standard solution with a series of diluted concentration. All the dilution processes were performed via a diluter dispenser (Microlab 600 series, Hamilton). Details of dilution folds are listed in Table S1. Plasma gas of argon with 10.00 l/min in velocity was generated from radio frequency power of 1.20 kW, auxiliary and carrier gas of argon was 0.60 and 0.70 l/min, respectively. The time for exposure, solvent rinse and sample rinse was 30, 30

and 45 sec, respectively. A detection wavelength of 220 nm yielded relative standard deviation (RSD) below 1.2% for three times measurements of each sample. The background was well corrected and the range for integration was properly selected. A calibration curve of the standard solution series was established by linear fitting with correlation coefficient better than 0.997. Digested QDs solution was estimated according to this curve, and mole concentration of PbS was calculated for the colloid PbS QDs solution.

Table S2. Details of ICPE results and calculated mole concentration of PbS according to detection wavelength of 220 nm

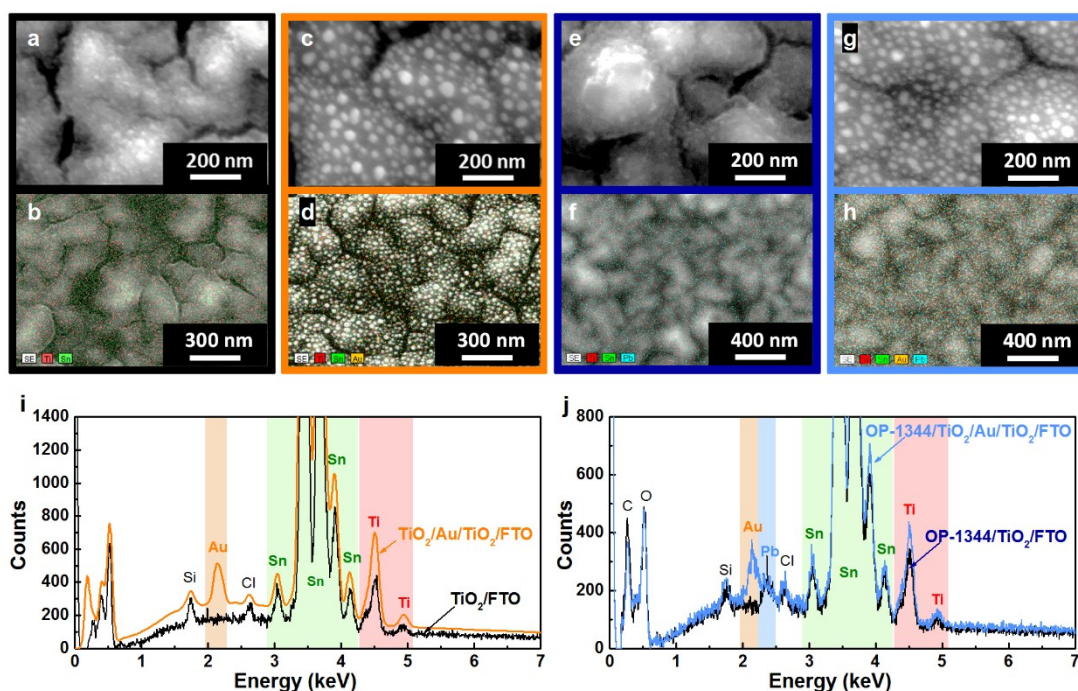
Sample file	Diluted conc. ppm	Average a.u. □	RSD %
cal1	0.250	290.55	1.76
cal2	0.500	454.03	0.40
cal3	0.714	598.57	0.37
cal4	1.000	802.75	0.21
cal5	1.250	949.72	0.10
cal6	1.429	1072.98	0.29
cal7	1.667	1231.75	0.53
cal8	1.818	1340.37	0.60
cal9	2.000	1446.98	0.46
cal10	2.273	1637.88	0.33
cal11	2.500	1777.23	0.57
cal12	2.778	1948.81	0.11
cal13	3.125	2160.35	0.18
cal14	3.333	2304.23	0.36

Table S3 Calculated mole concentration of PbS

Sample	Average a.u. □	SD	RSD %	Calculated Pb Conc. ppm	Mole Conc. of PbS in original solution umol/mL	Number of QDs per mL mL <sup>-1</sup>
OP-728	1031.49	0.43	0.04	1.37	132.112	$7.16 \times 10^{17}$
OP-1101	808.60	3.30	0.41	1.03	99.164	$1.05 \times 10^{16}$
OP-1344	642.08	0.64	0.10	0.77	74.549	$2.83 \times 10^{17}$

## SEM image & EDS mapping spectrum

Bare titanium dioxide and plasmonic substrates before and after the sensitization of PbS QDs were measured via scanning electron microscopy (SEM) equipped with energy-dispersive X-ray spectroscopy (EDS) at The University of Manchester. Figure S1 gives the details of SEM image (top row, 250,000x, 10 kV), EDS element mapping images (middle row, 62,500x, 20 kV) and the corresponding spectrum (bottom row) of TiO<sub>2</sub> (black column), TiO<sub>2</sub>/Au/TiO<sub>2</sub> (orange column), OP-1344/TiO<sub>2</sub> (navy column) and OP-1344/TiO<sub>2</sub>/Au/TiO<sub>2</sub> (blue column). SEM images show that gold nanoparticles (Au NPs), with an average diameter around 20 nm, are well dispersed on the TiO<sub>2</sub> surface without dissolution even after deposition of PbS QDs according to SEM images. Element mapping by EDS illustrates the uniform distribution of Ti (red) and Sn (green, coming from the FTO glass (F doped SnO)) elements on bare TiO<sub>2</sub> substrate, Au (orange) on plasmonic substrate and Pb (blue) on sensitized substrate. EDS spectrums based on the element mapping identify the existence of Au around 2.1 keV (orange area) in comparison with bare TiO<sub>2</sub> substrate, as well as the existence of Pb element at 2.34 keV (azure area) after sensitization even in the resolution limitation of SEM for the PbS QDs with average diameter less than 5 nm. PbS QDs was loaded 5 times of the maximum amount for the photocurrent measurements in order to get significant counts for EDS. The EDS maps displayed an even distribution of Pb across the dropcasted films indicating the PbS QDs are evenly distributed.



**Figure S1.** SEM images (top row), EDS mapping images (middle row) and corresponding spectrum (bottom row) of bare titanium dioxide and plasmonic electrode before and after sensitized by OP-1344 QDs. **a, b**, TiO<sub>2</sub>, **c, d**, TiO<sub>2</sub>/Au/TiO<sub>2</sub>, **e, f**, OP-1344/TiO<sub>2</sub> and **g, h**, OP-1344/TiO<sub>2</sub>/Au/TiO<sub>2</sub> substrate. **i, j**, EDS spectrum of TiO<sub>2</sub> and TiO<sub>2</sub>/Au/TiO<sub>2</sub> substrate before and after sensitized by OP-1344 QDs. Element mapping involved in gold M<sub>α</sub> (orange), lead M<sub>α</sub> (blue), titanium K<sub>α</sub> (red) and tin L<sub>α</sub> (green, coming from FTO glass) emission (PbS particle density:  $5.5 \times 10^{12} \text{ cm}^{-2}$ ). The dark area in **g** indicates

the formation of multiple layers in the sunken region of FTO glass by loading a large density of QDs.

### Extinction spectrum & size distribution of Au NPs

UV-vis spectrum of Au NPs deposited on TiO<sub>2</sub> film was recorded by Multi Channel Photo Detector MPD-311C and UV-vis light source MC-2530 system (Otsuka Electronics Co., Ltd.), with a spectral resolution of 1 nm. The light source produces an irradiation area of 0.3 cm<sup>2</sup>. Au NPs present a peak maximum of LSPR around 580 nm in the range of 1.8~2.5 eV, as marked in the yellow area. The size of the Au NPs was confirmed to be 20.6 ± 6.3 nm according to the SEM image of the Au/TiO<sub>2</sub> substrate.

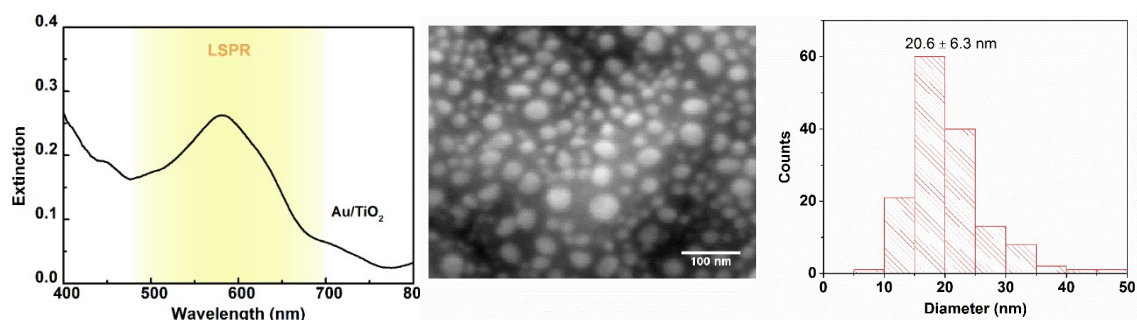


**Figure S2.** Characterization of Au/TiO<sub>2</sub> substrate: (left) extinction spectrum, (middle) SEM image and (right) its size distribution. The yellow area in the extinction spectrum illustrates the LSPR region.

### TEM image & size distribution of PbS QDs

Synthesized colloidal PbS QDs were diluted in hexane and dispersed onto copper grid coated with a holey carbon film. The TEM characterizations were performed using a FEI-Tecnai F30 at The University of Manchester, operated at 200 kV at a magnification of 450,000x. The size of the QDs were confirmed to be  $4.8 \pm 0.4$  nm,  $3.9 \pm 0.4$  nm and  $2.0 \pm 0.3$  nm for OP-1344, OP-1101 and OP-728, respectively. The diameter results measured via TEM are consistent with the estimated results of 4.8, 3.7, and 2.3 nm via the absorption spectra.

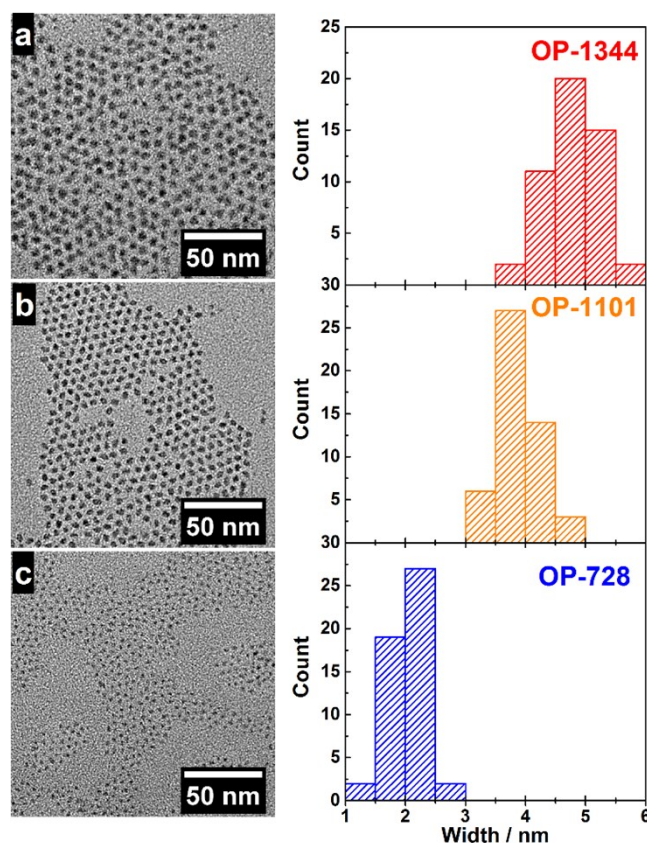


**Figure S3.** TEM images of colloidal PbS QDs (left) and their size distribution (right): a, OP-1344, b, OP-1101 and c, OP-728.

### Size-dependent energy position

The PbS QDs were named according to the absorption maximum corresponding to the 1<sup>st</sup> exciton peak wavelength as OP-1344, OP-1101 and OP-728 respectively. Their average bandgap ( $E_g$ ) were determined by the 1<sup>st</sup> exciton peak, giving 0.9, 1.1 and 1.7 eV from infrared to visible light. The average diameters were estimated to be 4.8, 3.7 and 2.3 nm in diameter, respectively. Within the Bohr radius of 18 nm, all these PbS QDs exhibit strong quantum confinement. The size-dependent energy positions of the valence band (VB) and conduction band (CB) of PbS QDs were calculated according to the ionization energy and values of bulk PbS ( $E_g=0.41$  eV,  $E_{CB}=-0.29$  V,  $E_{VB}=0.12$  V (vs. Ag/AgCl)).<sup>2</sup> The flat-band potential ( $U_{FB}$ ) of anatase TiO<sub>2</sub> prepared by the LPD method is around -0.63 V (vs. Ag/AgCl) in neutron solution according to the previous study of thin TiO<sub>2</sub> film with thickness of 150 nm.<sup>3</sup> Only the energy position in neutron solution is illustrated to compare the band-

edge alignment for the reason that not only TiO<sub>2</sub> but also PbS present the same band-edge shift towards negative direction<sup>4</sup> in the alkane electrolyte (cal. 0.059 V/pH at 298 K<sup>5-7</sup>). Strong quantum confinement enlarges the CB of OP-728 to a more negative potential than the  $U_{FB}$  of TiO<sub>2</sub> whereas the CB of infrared OP-1344 is almost the same as the  $U_{FB}$  of TiO<sub>2</sub>, indicating electron injection from excited OP-728 is much easier rather than the two others.

Table S4 Estimated MEG threshold of each size QDs

QDs	1 <sup>st</sup> Exciton	Half-width	Bandgap ( $E_g$ )		MEG Threshold			MEG Threshold	
		nm	eV	error	(energy, $2.6E_g$ )	error	(wavelength)	error	
					eV		nm		
<b>OP-728</b>	728	60	1.70	± 0.14	4.43	-0.40 0.34	280	± 23	
<b>OP-1101</b>	1101	55	1.13	± 0.05	2.93	-0.15 0.14	423	± 21	
<b>OP-1344</b>	1344	62	0.92	± 0.04	2.40	-0.12 0.11	517	± 24	

### Photoelectrochemical measurements

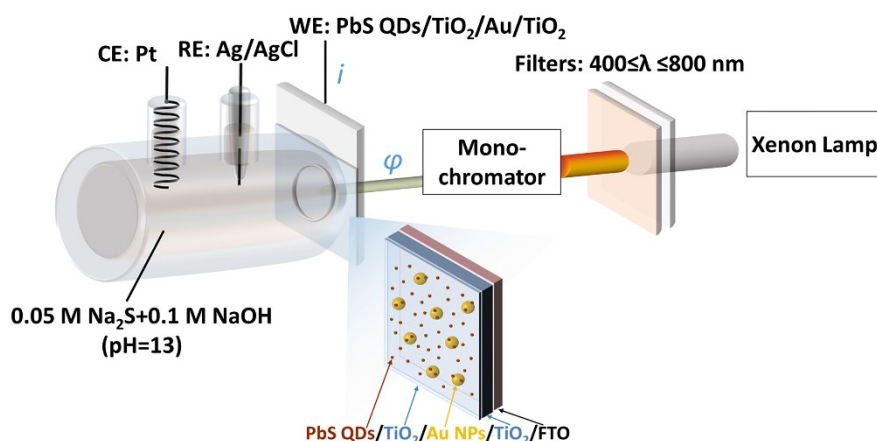


**Figure S4.** Schematic illustration of photoelectrochemical measurement using three-electrode system using PbS QDs/TiO<sub>2</sub>/Au/TiO<sub>2</sub> electrode in contact with S<sup>2-</sup>/S<sub>n</sub><sup>2-</sup> redox couple under potential control referred to Ag/AgCl (sat. KCl) reference electrode.

### Steady-state on-off reactions

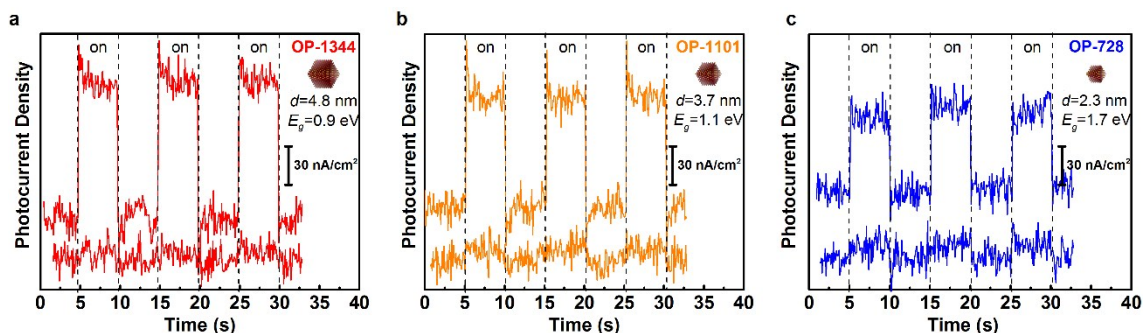


**Figure S5.** Measured photocurrent of **a**, OP-1344 **b**, OP-1101 and **c**, OP-728 sensitized TiO<sub>2</sub>/Au/TiO<sub>2</sub>

(upper) and  $\text{TiO}_2$  (down) under irradiation of 520 nm based on steady state on-off response at -0.1 V in electrolyte of 0.05 M  $\text{Na}_2\text{S}$ +0.1 M NaOH. Baseline due to exchange current was subtracted. Inset: enlarged view of on-off response irradiated at 510 nm. Noise width is around 5 nA.

### Potential-dependent electron injection

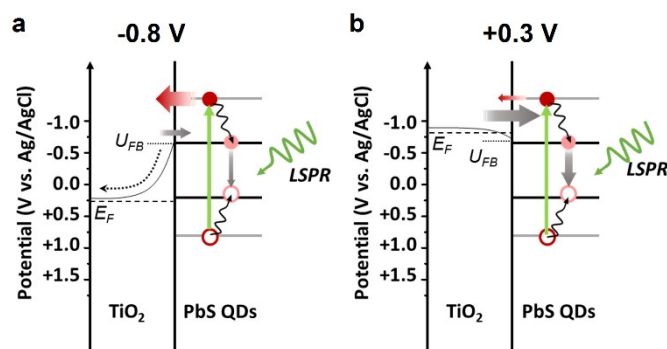


**Figure S6.** The energy diagram of PbS QDs-sensitized  $\text{TiO}_2$  electrodes at the applied electrochemical potential of **a**, -0.8 and **b**, 0.3 V, respectively. Hot electron injection (red thick arrows) and electron-hole pair recombination (grey thick arrows)

### Error evaluation

As mentioned in the manuscript (Fig.3) and illustrated in Fig. S7, onset potential was evaluated as the electrochemical potential (point b) at 10% of the photocurrent density measured at 0.5 V (point  $J_B$ ) and irradiated at each irradiated wavelength. The error of photocurrent density (blue ribbon shadow) was calculated from the noise signal of each measured photocurrent (see Fig. S5). B-spline function was used to fit all the photocurrent densities and errors. Thus the error of onset potential was evaluated as the electrochemical potential (point a and c) at 10% of the errors of the photocurrent density measured at 0.5 V (point  $J_A$  and  $J_C$ ).

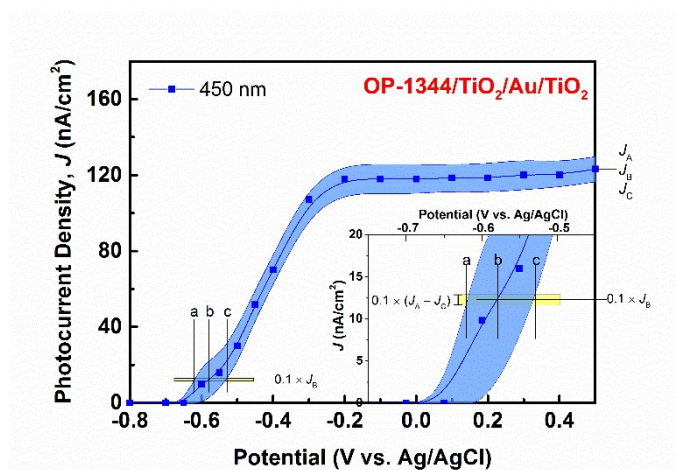


**Figure S7.** Error evaluation of onset potential. OP-1344 sensitized  $\text{TiO}_2/\text{Au}/\text{TiO}_2$  substrates irradiated at 450 nm. The mole number densities of PbS is  $0.5 \text{ nmol cm}^{-2}$ .

## Onset potential

There is a deviation in the values of  $\phi_{\text{onset}}$ , at respective experiments due to inhomogeneity in the distribution of loaded QDs on nanostructured electrodes prepared by the drop-casting method. To clarify the distribution of the values as well as the general tendency in the shift of  $\phi_{\text{onset}}$ , the dependence of the QDs loading amounts on photocurrent generation was observed by varying from 0.25, 0.5 to 1.0 nmol/cm<sup>2</sup>.

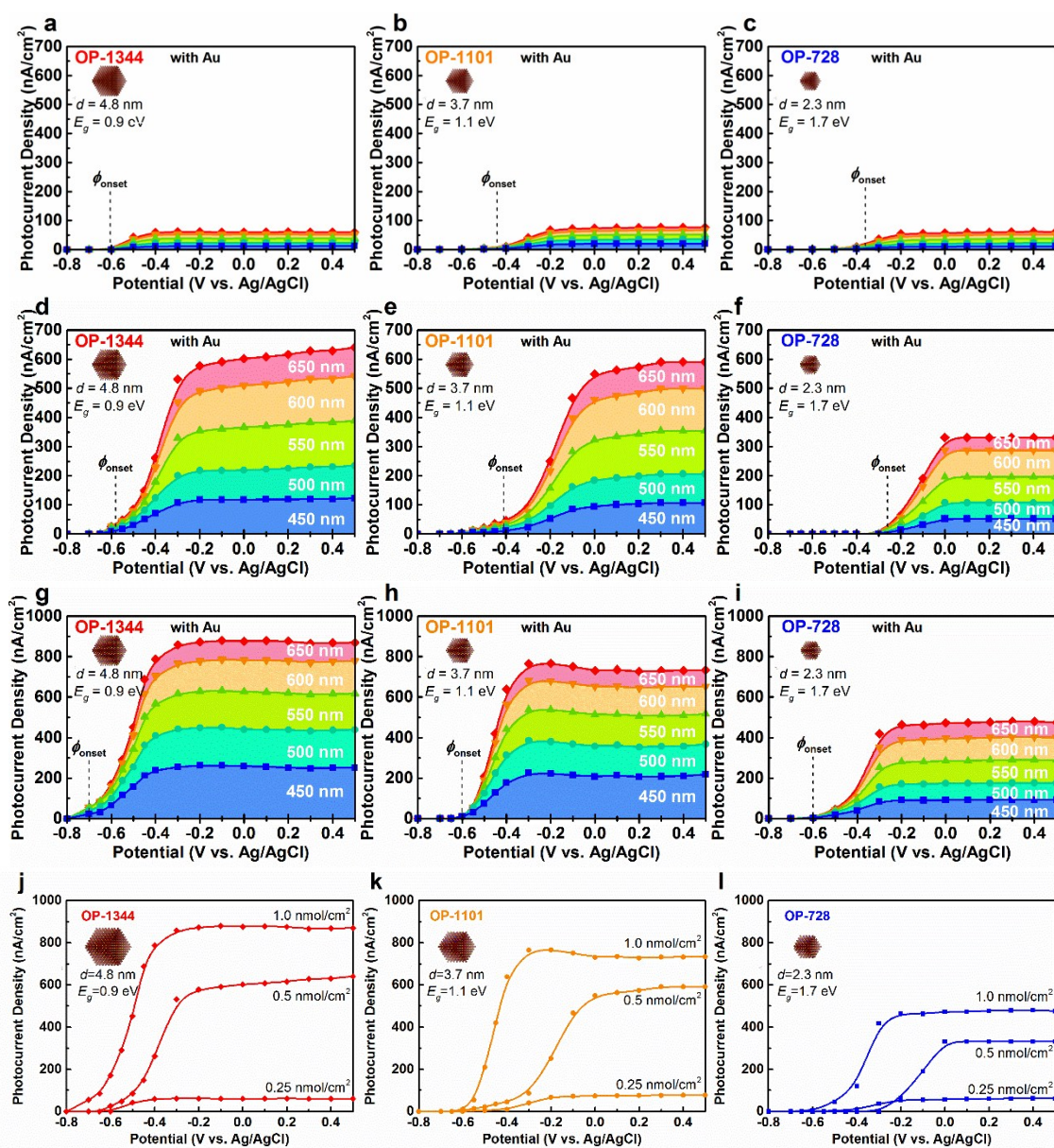


**Figure S8.** Stacked area charts of size-dependent photocurrent generation of **a, d, g**, OP-1344, **b, e, h**, OP-1101 and **c, f, i**, OP-728 sensitized TiO<sub>2</sub>/Au/TiO<sub>2</sub> substrates irradiated at 450 (blue), 500 (cyan), 550 (green), 600 (orange), and 650 (red) nm, in the potential range from -0.8 V to 0.5 V vs. Ag/AgCl in the electrolyte of 0.05 M Na<sub>2</sub>S and 0.1 M NaOH. The mole number densities of PbS are respectively 0.25 nmol cm<sup>-2</sup> for a-c, 0.5 nmol cm<sup>-2</sup> for d-f, and 1.0 nmol cm<sup>-2</sup> for g-i. Vertical dashed lines present

the onset potential ( $f_{\text{onset}}$ ) corresponding to the electrochemical potential at 10% of the photocurrent density measured at 0.5 V and irradiated at 450 nm. **j, k, l**, Loading amount dependent photocurrent density summarized from **a-i**.

### Calculation of output power density

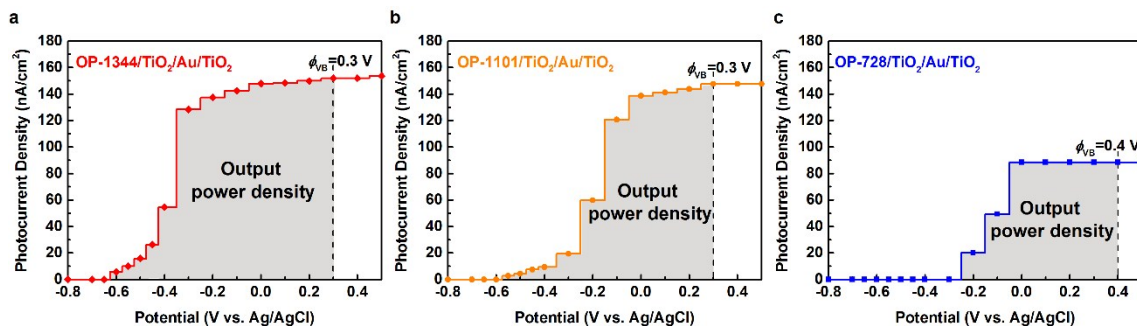


**Figure S9.** Calculated output power density (grey area). **a**, OP-1344, **b**, OP-1101 and **c**, OP-728 as the area integral of photocurrent density at each potential upon valence band ( $\phi_{\text{VB}}$ ) at irradiation of 500 nm. The mole number density of PbS is all around 0.5 nmol/ cm<sup>-2</sup>.

## Internal Quantum Efficiency

Internal quantum efficiency (absorbed photon-current efficiency, APCE) was calculated by the following equation:

$$IQE\% = \frac{N_e}{N_{photon}} \times 100$$

where  $N_e$  is the number of electrons generated by per QD per second per  $cm^2$

$$N_e = \frac{J}{q}$$

and  $N_{photon}$  is the number of photons absorbed by per QD per second per  $cm^2$

$$N_{photon} = \frac{P}{hc / \lambda} \cdot Abs$$

with constants of elementary charge  $q$  ( $1.60217657 \times 10^{-19}$  C), Planck's constant  $h$  ( $6.62606947 \times 10^{-34}$  J·sec), speed of light  $c$  ( $299792458$  m/s), and irradiation wavelength  $\lambda$  in meter; and measured quantities of photocurrent density  $J$  in ampere per  $cm^2$ , incident power density  $P$  in watts per  $cm^2$ , and fraction of incident light absorbed by QDs on the substrate under irradiation  $Abs$ .

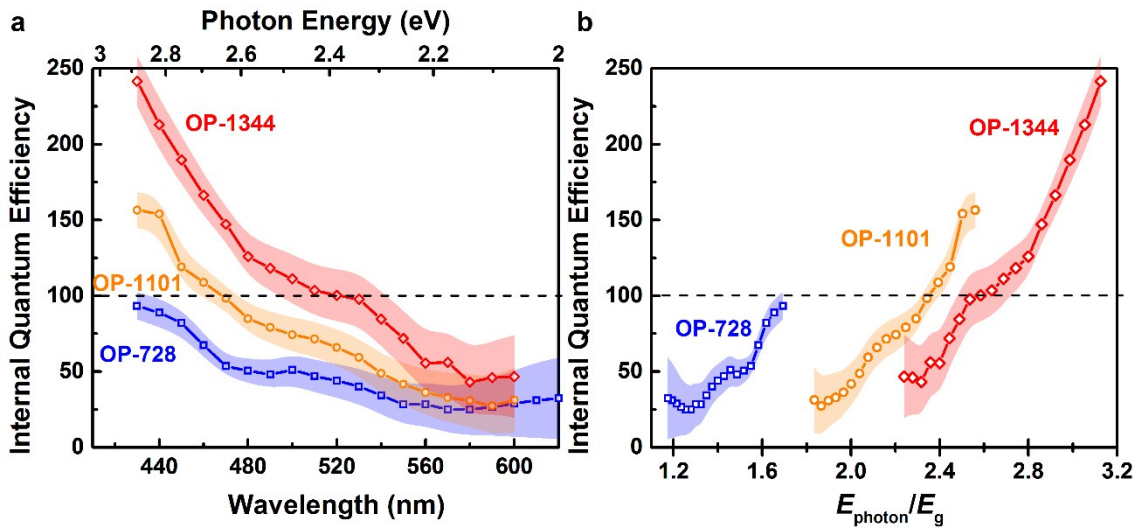


**Figure S10.** Internal quantum efficiency of bare titanium dioxide sensitized by OP-728 (blue), OP-1101 (orange) and OP-1344 (red) PbS QDs as a function of **a**, wavelength and **b**, photon energy normalized by the sample band gap. Areas present error bar including uncertainty of quantity analysis, photocurrent noise width and wavelength-dependent absorbance. Dashed lines illustrate the IQE=100%. PbS particle densities within a single layer domain are  $2.6 \times 10^{12}$ ,  $5.9 \times 10^{11}$  and  $2.7 \times 10^{11} cm^{-2}$ , respectively. The mole number density of PbS is all around  $0.5 nmol/cm^2$ .

## IPCE and EF changes depending on the amount of PbS QDs loading

The LSPR coupling effect was evaluated by increasing loading amounts of PbS QDs. The enhanced IPCE of TiO<sub>2</sub>/Au/TiO<sub>2</sub> to TiO<sub>2</sub> substrates gives the EF of these electrodes. As the quantity of PbS QDs increased up to a loading of  $1.1 \times 10^{13}$ ,  $2.4 \times 10^{12}$ , and  $1.1 \times 10^{12}$  cm<sup>-2</sup>, respectively for OP-728, OP-1101, and OP-1344 on both TiO<sub>2</sub>/Au/TiO<sub>2</sub> and TiO<sub>2</sub> substrates, the IPCE increased as a whole over the observed wavelength region. With increased loading, the IPCE of TiO<sub>2</sub>/Au/TiO<sub>2</sub> in the LSPR wavelength region first increases and then saturates, while the EF decreased. This suggests a low loading amount improves the coupling between PbS QDs and Au NPs. The maximum EF values obtained were 28 and 37 for OP-728 and OP-1101 at 590 nm and 33 for OP-1344 at 580 nm, respectively, with PbS QDs density of  $2.6 \times 10^{12}$ ,  $5.9 \times 10^{11}$ , and  $2.7 \times 10^{11}$  cm<sup>-2</sup> (the mole number densities of PbS are all near 0.5 nmol cm<sup>-2</sup>). Considering the number of PbS QDs needed to cover the ideal flat substrate with a close-packed single layer is  $9.3 \times 10^{13}$ ,  $3.4 \times 10^{13}$ , and  $2.0 \times 10^{13}$  cm<sup>-2</sup>, roughly 2% coverage of PbS QDs is appropriate to prepare the plasmon-enhanced photocurrent generation system. The reason that a sparse QD distribution improves the enhancement was ascribed to distance-dependent plasmon coupling<sup>8</sup>. As the loading amount increases, the formation of multiple layers becomes inevitable (Figure 1g), and the stacked PbS QDs with a distance exceeding the effective LSPR spatial region cannot couple well with the Au NP. In this sense, optimization of the QD loading amounts is crucial to monitor the LSPR effect in the plasmon-enhanced photocurrent generation system.

The enhancement factor (EF) was introduced. In the present experiment, as the loading amounts of PbS QDs both on the substrates with and without Au were carefully controlled to be the same, EF was calculated as the yielded IPCE of PbS QDs/TiO<sub>2</sub>/Au/TiO<sub>2</sub> substrate (with Au NPs) to PbS QDs/TiO<sub>2</sub> substrate (without Au NPs) at a certain wavelength, as described below.

$$\text{Enhancement Factor} = \frac{\text{IPCE}_{\lambda, \text{w/Au}}}{\text{IPCE}_{\lambda, \text{w/oAu}}}$$

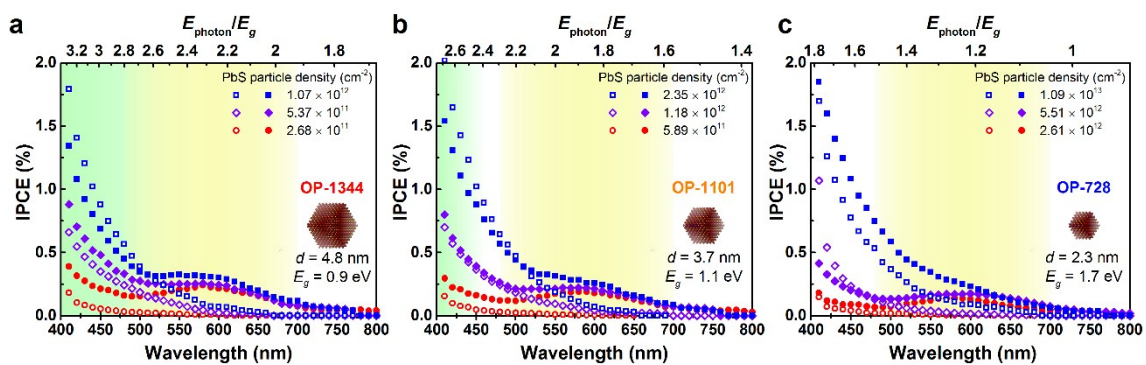


**Figure S11.** Comparison of IPCE changes depending on the loading amount of **a**, OP-1344, **b**, OP-1101 and **c**, OP-728-sensitized TiO<sub>2</sub> (hollow scatter) and TiO<sub>2</sub>/Au/TiO<sub>2</sub> (solid scatter) measured at -0.1 V in electrolyte of 0.05 M Na<sub>2</sub>S+0.1 M NaOH. The mole number densities of PbS are respectively 0.5 nmol cm<sup>-2</sup> (red circles), 1.0 nmol cm<sup>-2</sup> (purple diamonds), and 2.0 nmol cm<sup>-2</sup> (blue square).

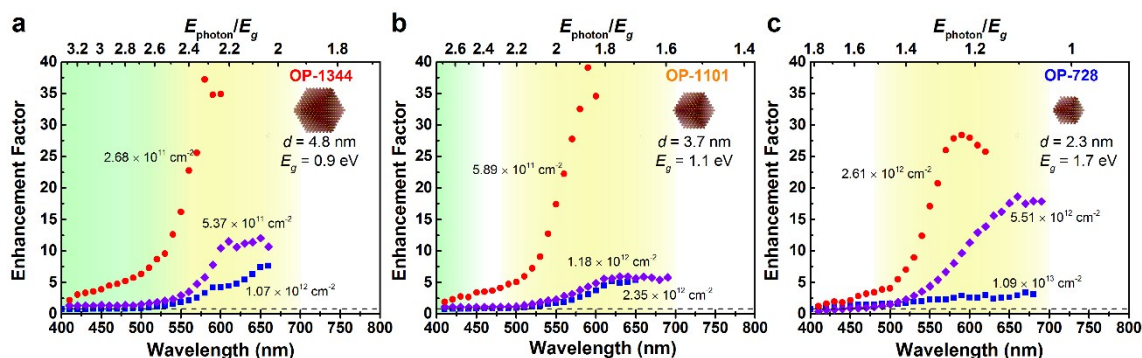


**Figure S12.** Comparison of the enhancement factor changes depending on the loading amount of **a**, OP-1344, **b**, OP-1101 and **c** OP-728, measured at -0.1 V in electrolyte of 0.05 M Na<sub>2</sub>S+0.1 M NaOH. The mole number densities of PbS are respectively 0.5 nmol cm<sup>-2</sup> (red circles), 1.0 nmol cm<sup>-2</sup> (purple diamonds), and 2.0 nmol cm<sup>-2</sup> (blue square).

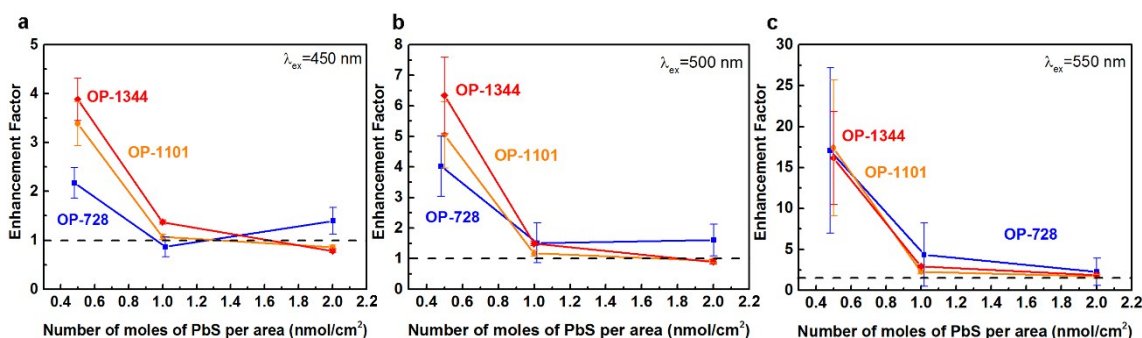


**Figure S13.** Comparison of loading amount dependent enhancement factor of PbS QDs at different wavelength light irradiation of **a**, 450 nm, **b**, 500 nm and **c**, 550 nm.

### Finite-difference time-domain (FDTD) simulations

Finite difference time domain method (FDTD) of solving Maxwell equations was used to calculate nanoparticles extinction and electromagnetic field distribution. A commercial software, EEM-FDM (Ltd. EEM, Japan), was employed to carry out FDTD analysis for Au NP-PbS QD coupling system. Wavelength-dependent optical constants of bulk Au and bulk PbS were taken from the references.<sup>9, 10</sup> The systems were illuminated with a s-polarized plane wave with the electric field amplitude of 1 V/m. Boundary condition of perfectly matched layers (PMLs) were used to absorb the scattered radiation in all directions. The environment was set as the vacuum. Meshes were set sufficiently small in order to calculate local-field enhancements with sufficient spatial resolution; the details are listed as the following: 0.2 nm in the gap of Au NP-PbS QD as well as the space containing PbS QDs, 0.5 nm for the space containing bulk Au sphere, and 1 nm for the vacuum domain. The field was calculated as the ratio of its value at a given point relative to the incident field,  $|E|/|E_0|$ .

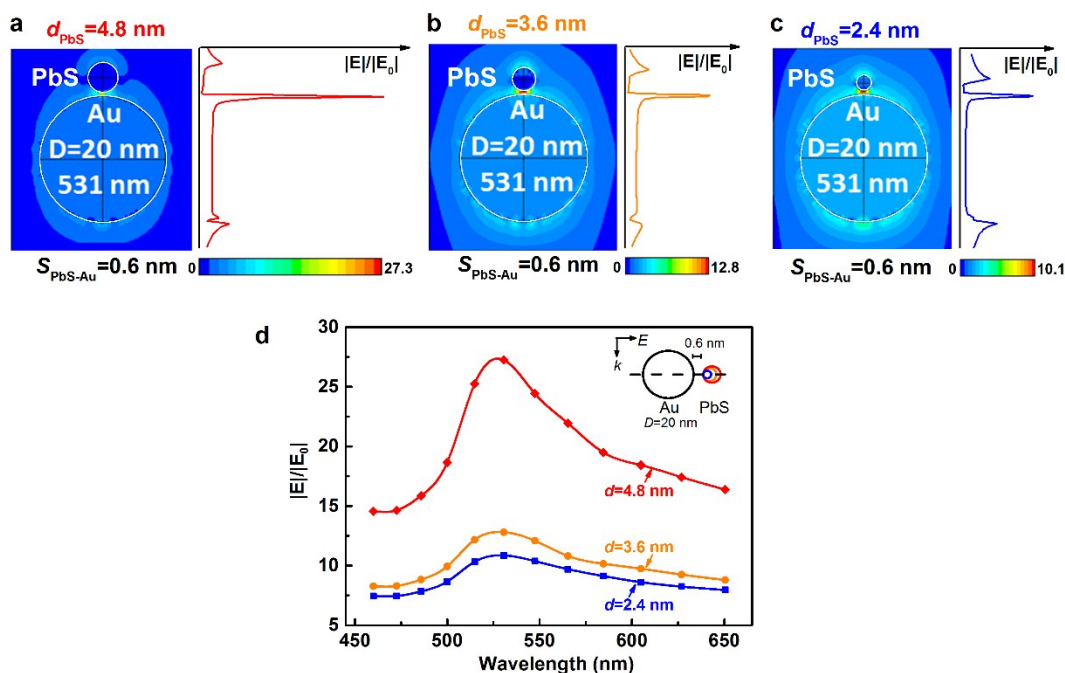


**Figure S14. Results of FDTD simulation for Au-PbS hetero-system.** PbS QDs with the diameter of **a**, 4.8 nm **b**, 3.6 nm and **c**, 2.4 nm, spaced 0.6 nm from Au NP of 20 nm under irradiation of 531 nm. Contour plot: electric-field distribution excluding the incident field; line plot: the corresponding spatial electric-field distributions along the center line connecting Au NP and PbS QD (white dashed line). **d**, Wavelength-dependent maximum value of the electric field between the gap along the center line of the Au-PbS hetero-system.

## References

1. Oh, J. K.; Lee, J. Y.; Lee, H. Y.; Kim, S. G.; Han, C.; Shin, J. K. *Geosystem Engineering* **1999**, 2, (1), 1-6.
2. Jasieniak J, Califano M, Watkins ES. Size-Dependent Valence and Conduction Band-Edge Energies of Semiconductor Nanocrystals. *ACS nano* **2011**, 5 (7): 5888–5902.
3. Kavan, L.; O'Regan, B.; Kay, A.; Grätzel, M. *J. Electroanal. Chem.* **1993**, 346, (1), 291-307.
4. Xu, Y.; Schoonen, M. A. A. *Am. Mineral.* **2000**, 85, (3-4), 543-556.
5. Kavan, L.; Grätzel, M.; Gilbert, S. E.; Klemenz, C.; Scheel, H. J. *J. Am. Chem. Soc.* **1996**, 118, (28), 6716-6723.
6. Beranek, R. *Adv. Phys. Chem.* **2011**, 2011, 20.
7. Beranek, R. *Advances in Physical Chemistry* **2011**, 2011.
8. Kawawaki, T.; Takahashi, Y.; Tatsuma, T. *J. Phys. Chem. C* **2013**, 117, (11), 5901-5907.
9. Johnson, P. B.; Christy, R. W. *Phys. Rev. B* **1972**, 6, (12), 4370-4379.
10. Palik, E. D., *Handbook of Optical Constants of Solids*. Academic Press: New York, 2011; p 187-227.